J. Inst. Eng. India Ser. B (December 2020) 101(6):631–639
https://doi.org/10.1007/s40031-020-00478-1

ORIGINAL CONTRIBUTION

# Detailed Study of Solar Energy Conversion System using Boost Converter—a New MPPT Technique

**CH. S. Balasubrahmanyam[1] · Om Hari Gupta[1]**

Received: 20 December 2019 / Accepted: 7 August 2020 / Published online: 18 August 2020


**Abstract** Recent expansions in the emerging technologies have enlarged the consumption of electric power enormously which, conventionally, leads to the installation of power plants of huge capacity. So, to meet the electric power demand, the usage of renewable energy resources has become predominant in the present scenario. Solar photovoltaic energy conversion system that converts solar irradiance directly into electrical energy is a great opportunity among the available renewable energy resources as it is very abundant. In this paper, the key objective is to elucidate the detailed procedure of the maximum power-point tracking process for the solar panel with both stand-alone and grid-connected solar energy conversion system using a boost converter. The proposed system is simulated using MATLAB/Simulink, and comparative analysis shows the better performance of the proposed scheme.

**Keywords** Boost converter · Maximum power-point tracking · Photovoltaic · Solar energy conversion system

**List of symbols**

| | |
|---|---|
| P&O | Perturb and observe. |
| MPPT | Maximum power-point tracking. |
| MPP | Maximum power point. |
| SECS | Solar energy conversion system. |
| NHS | Normal harmonic search. |
| HCC | Hysteresis current control. |
| PNKLMS | Power normalized kernel least mean square. |
| UAV | Unmanned aerial vehicle. |
| RBFN | Radial basis function network. |
| CPHO | Crowded plant height optimization. |
| SPEGS | Solar photovoltaic energy generation system. |
| PSO | Particle swarm optimization. |
| DS | Distributed sparse. |
| $I_o$ | Reverse saturation current of diode in amps. |
| $I_{pv}$ | Current from PV cell. |
| η | Diode ideality factor. |
| $V$ | Voltage across diode in volts. |
| $V_T$ | Thermal voltage in volts. |
| T | Temperature in kelvin (K). |
| q | Charge on electron, $1.6 \times 10^{-19}$ C. |
| FF | Fill factor. |
| $V_{mp}$ | Voltage of PV array at MPP. |
| $I_{mp}$ | Current of PV array at MPP. |
| $V_{oc}$ | Open-circuit voltage of PV array. |
| $I_{sc}$ | Short circuit current of PV array. |
| LS | Factor describing the boundary for low-slope region. |
| HS | Factor describing the boundary for high-slope region. |
| K | Factor multiplied to slope according to different regions. |
| d$D$ | Change in duty cycle. |

## Introduction

To match the ever-increasing need of power, the concept of renewable-based power generation is being implemented and a lot of research is being carried out on the same [1, 2]. With a new NHS MPPT technique, a single-phase two-

✉ Om Hari Gupta
omhari.ee@nitjsr.ac.in

[1] Department of Electrical Engineering, NIT Jamshedpur, Jamshedpur, India

stage system with storage connected to the grid is implemented in [3]. Here, the VSC is controlled using a new PNKLMS technique which also maintains the power quality. Further, any sensor for DC-link voltage measurement is not required [3]. Fuzzy logic-based MPPT technique for PV-based UAV is proposed in [4] which has a quick response in tracking the MPP with reduced oscillations and increased efficiency. An MPPT controller based on RBFN for both solar and wind generation systems is examined, and its performance is compared with the conventional MPPT algorithms. The scheme has an interesting advantage of decreasing the components in the hardware MPPT controller design [5]. An innovative CPHO regulated MPPT algorithm which includes an optimum duty cycle through a PI controller for boost converter is introduced in [6]. It works on the rule height convergence, and its performance is compared with conventional P&O technique. For partial shading condition (PSC), there will be multiple maximum power points, so a new overall distribution (OD) MPPT algorithm to rapidly search MPP and after being integrated with PSO algorithm to enhance accuracy is proposed in [7]. A grid-connected SPEGS is implemented in [8] which provides multi-functional deals with active power filtration and supports active power demand. Also, a new multi-purpose DS controller is used to get reference grid currents and to improve performance. SECS is mostly preferred due to its numerous advantages over other types of renewable-based energy conversion systems [9]. Major advantages are low maintenance cost, static generation, and being abundant in almost all over the world. Simultaneously, a lot of research is being carried out in the area of SECS [10–12]. The output of SECS depends on the irradiance and temperature. If the irradiance increases, the output will also increase and vice versa, while if temperature increases, the output decreases and vice versa. The I–V characteristics can be used to determine the exact variations in the solar output with the change in irradiance and temperature [13]. A technique called MPPT is used to extract maximum power under variable irradiance and temperature. There is a lot of literature available on MPPT for SECS. There are several existing techniques for MPPT, e.g., P&O [14], incremental conductance [15], constant voltage [16], current sweep [17], temperature measurement [18] methods, etc. The most used method is P&O due to its simplicity [19]. Other methods also have their benefits and limitations. For instance, the control logic of the incremental conductance method is complex for hardware implementation, the temperature measurement method does not include the effect of irradiance change, and so on. Therefore, there is still some scope for improvements in MPPT. Moreover, the basics of the SECS still need to be discussed in detail for a better understanding of the readers. A literature survey states that compared to buck and buck–boost converters, boost converter works at high efficiency and is good at tracking MPPT [20], [21].

This article presents a detailed study of the basics of stand-alone as well as grid-connected SECS with MPPT using a boost converter and also proposes a new MPPT technique. Furthermore, the newly proposed technique is compared with the conventional P&O technique. From the comparative analysis, it is found that the proposed method gives lesser oscillatory output than that of the P&O technique in stand-alone mode while providing better performance in grid-connected mode.

*Solar Energy Conversion Technique* The equivalent circuit of a solar cell—excluding the lossy components as they have a minor impact on the characteristics—is shown in Fig. 1a. The output current equation of the solar cell can be obtained using (1) and (2) and is given in (3).

$$I_{pv} = I_D + I \tag{1}$$

$$I_{pv} = I_o\left[e^{\frac{V}{\eta V_T}} - 1\right] + I \tag{2}$$

$$\text{Since } I_D = I_o\left[e^{\frac{V}{\eta V_T}} - 1\right]$$

$$I = I_{pv} - I_o\left[e^{\frac{V}{\eta V_T}} - 1\right] \tag{3}$$

The current $I_{pv}$ depends upon the irradiance and temperature, while the diode current $I_D$ depends on various other parameters including voltage and temperature. Moreover, for a constant irradiance and temperature, if the load $R_L$ is varied, the solar cell-voltage and current will vary in the manner as depicted in Fig. 1b—also known as the I–V characteristic of a solar cell. It can also be seen that there are two hatched areas: one due to maximum power point and another due to open-circuit voltage $V_{oc}$ and short circuit current $I_{sc}$. The ratio of these two areas is nothing but the fill factor (FF) of the solar cell and is given in (4). The typical value of the fill factor is greater than 0.8 for $V/V_T$ to be 20 [22]. In Fig. 1e, power output v/s voltage curves of the considered solar panel are shown with their respective MPPs for each irradiance.

$$FF = \frac{V_{mp}I_{mp}}{V_{oc}I_{sc}} \tag{4}$$

The value of the fill factor defines the power conversion efficiency of a solar cell [13]. This efficiency may reduce if the maximum power point has not been achieved. The MPPT can be achieved by controlling the effective value of load resistance $R_L$. A DC-to-DC converter can help to vary the effective value of load impedance offered to the solar cell or PV module. The selection of the type of converter depends upon the impedance corresponding to maximum power and actual load impedance. For example, if the load

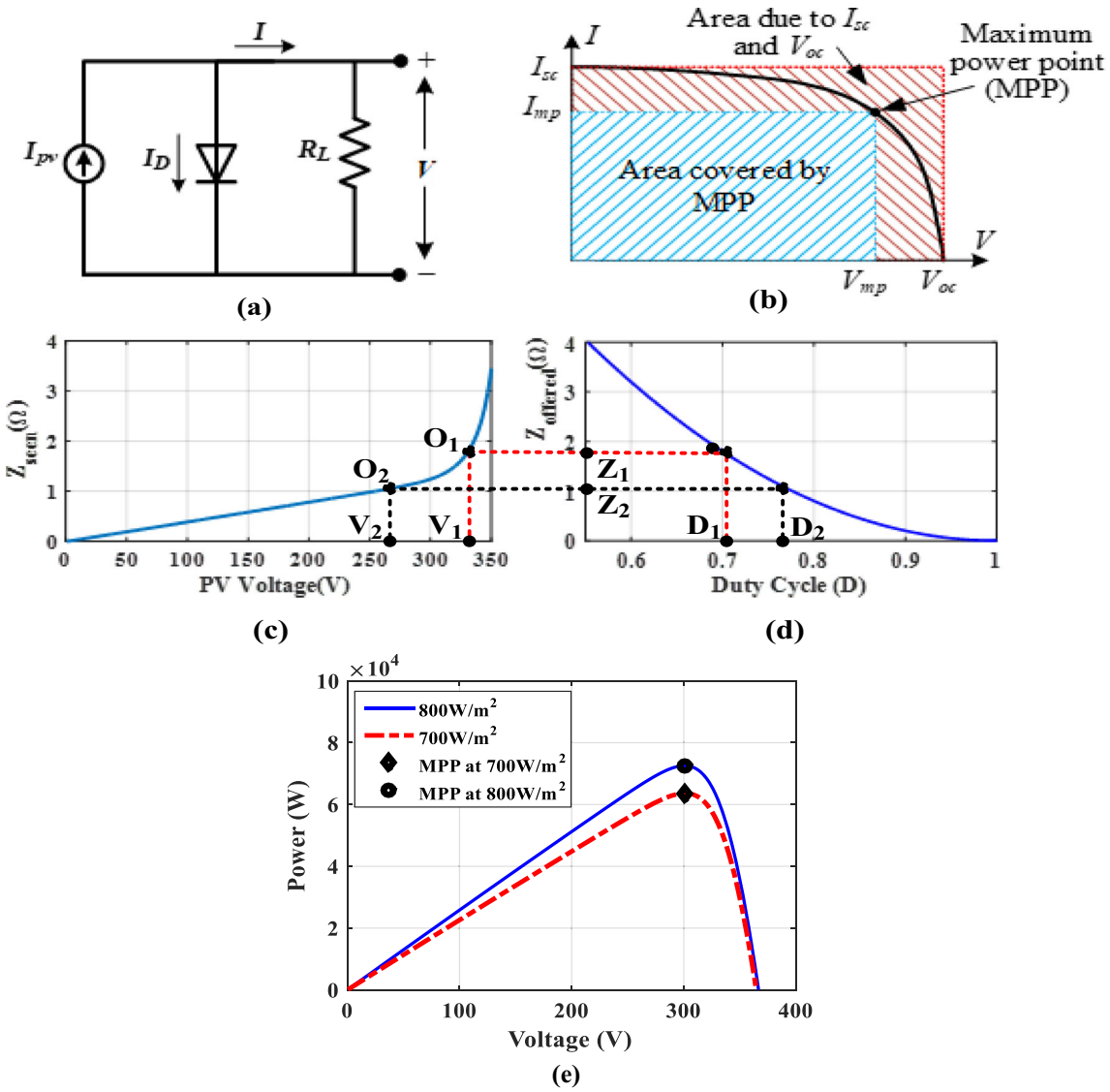


**Fig. 1** **a** Equivalent circuit of a PV cell; **b** I–V characteristic of solar cell and different areas; **c** plot of impedance of the PV array v/s voltage **d**; plot of impedance offered by boost converter v/s duty cycle; **e** power v/s voltage curves for irradiances 800 and 700 W/m$^2$ and their respective MPPs

impedance is, say, 20 Ω and impedance corresponding to a maximum power point (MPP) is 1.25 Ω, the boost converter should be used. On the contrary, if the load impedance is 12.5 Ω and impedance corresponding to MPP is 20 Ω, the buck converter should be used. The buck–boost converter has the capability of both. However, in most of the cases when irradiance is more, the impedance corresponding to MPP is less than the load impedance [23]. Therefore, either boost or buck–boost converter can be used. But since boost converter has higher efficiency and greater control over the range than buck–boost converter [20] and good tracking performance than buck converter [21], it is used in this study for maximum power-point tracking. According to the I–V curve of the PV array, the impedance seen by the photovoltaic (PV) array $Z_{seen}$ is calculated using (5).

$$Z_{seen} = \frac{V}{I} \tag{5}$$

In the I–V curve, when the PV output voltage is increasing, the PV output current decreases gradually up to the MPP. After the MPP, current decreases drastically. Therefore, the $Z_{seen}$ v/s PV output voltage plot, as shown in Fig. 1c, is nearly linear up to MPP, but after that, the impedance increases drastically because the PV voltage increases and the PV current decreases rapidly. Further, the impedance offered by the boost converter, i.e., $Z_{offered}$, with the change in duty cycle $D$ is given in (6) and plotted in Fig. 1d. By observing Fig. 1d, it can be said that the

variable impedance offered by the boost converter $Z_{offered}$ will be less than the load impedance as given in (7).

$$Z_{offered} = Z_L(1-D)^2 \tag{6}$$

$$Z_{offered} \leq Z_L \tag{7}$$

Now, using the I–V characteristic, Z–V characteristic can be obtained since impedance $Z_{seen}$ is nothing but the ratio of voltage $V$ and current $I$. Normally, to obtain the MPP, the search is done by varying impedance using the duty cycle of the converter. Figure 1c, d depict the impedance obtained from the I–V characteristic $Z_{seen}$ and impedance offered by the boost converter $Z_{offered}$ for a representative case. The relation between $Z_{offered}$ and $D$ is approximately inverse and the maximum impedance that the converter can offer to the solar panel is equal to the load impedance as D can be varied from 0 to 1—refer (6). Therefore, to increase the impedance offered by the converter, the duty cycle of the converter must be decreased. Now, suppose the operating point of the PV module is at $O_1$ as shown in Fig. 1c. At this operating point, the impedance offered by the converter is $Z_1$ corresponding to duty cycle $D_1$ and the PV module voltage is $V_1$. To get the operating point shifted to $O_2$—for the extraction of maximum power, the PV voltage should be shifted to $V_2$. That can be done by changing $Z_{offered}$ to $Z_2$ with the help of changing the duty cycle to $D_2$. Figure 2 includes the block diagram of a typical SECS. The PV array converts the sunlight into an electrical signal (DC). This DC output of the PV array is given to the boost converter to implement the MPPT. The MPPT controller measures the voltage and current of the PV array and generates the duty cycle for the boost converter. An inverter is usually connected after the boost converter to convert DC into AC. A capacitor is placed at DC bus to avoid the effect of fluctuations due to switching events. The inverter controller usually controls the output power to keep the capacitor voltage constant. In this study, both stand-alone mode and grid-connected mode are implemented separately. The circuit breaker is represented by switch $S_1$ which can be used to connect/disconnect the grid.

## Proposed MPPT Technique

First, the P–V curve of the solar panel is categorized into three regions based on the calculation of slope (dP/dV). The three regions are:

1. Low-slope region;
2. Medium-slope region;
3. High-slope region.

By observing the three regions shown in Fig. 3a, the MPP lies in the low-slope region. MPP is the intersection point of the +ve slope and −ve slope portions of the P–V curve. P–V curve varies with the variations in irradiance and temperature—accordingly, MPP gets shifted as represented earlier in Fig. 1e. Hence, the adopted MPPT technique must recognize the change in irradiance and temperature and consequently track the MPP on the P–V curves. The flowchart illustrates the proposed MPPT technique is shown in Fig. 3b. The objective is to obtain $I_{mp}$ and $V_{mp}$ of PV array—corresponding to maximum power for particular irradiance and temperature. Since the proposed MPPT technique works on the division of the P–V curve into different regions, the algorithm starts by calculating the change in voltage d$V$, change in power d$P$ and slope d$P$/d$V$. Then, if either the change in voltage or the change in power is zero, it indicates that MPP is reached, and if it is not zero, the voltage must be increased or decreased using the duty cycle $D$ of the converter. Equation (8) represents the updated duty cycle $D$ where $D1$ is the old duty cycle and d$D$ is the change in duty cycle. The term d$D$ is calculated by $\mathrm{d}D = K * \left(\frac{\mathrm{d}P}{\mathrm{d}V}\right)$, where $K$ is the factor multiplied to slope value according to the regions that are illustrated in Fig. 3a. The regions are divided based on the calculation of slope d$P$/d$V$. For the low-slope region, the slope value is less than $LS$, and for medium-slope region, it is between $LS$ and $HS$. For the high-slope region, the slope value will be greater than $HS$. For every iteration, the absolute value of calculated slope d$P$/d$V$ is compared with the predefined $LS$ or $HS$. When the operating point is close to MPP (i.e., low-slope region), the changes in duty cycle d$D$ should be small, and when it is away from MPP (i.e., medium-slope region), d$D$ should be larger. A small

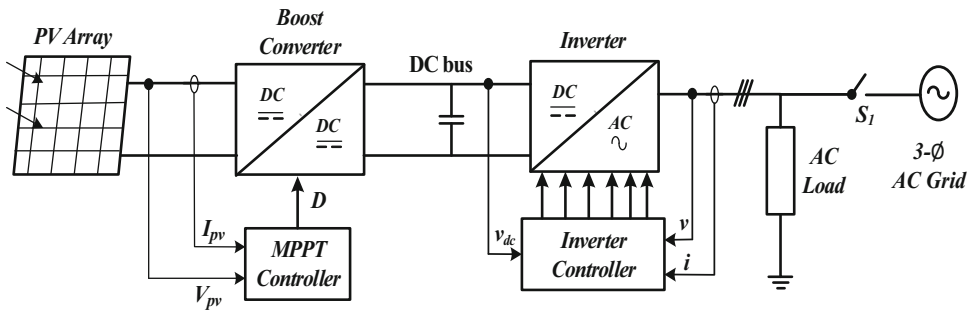


**Fig. 2** Block diagram of SECS

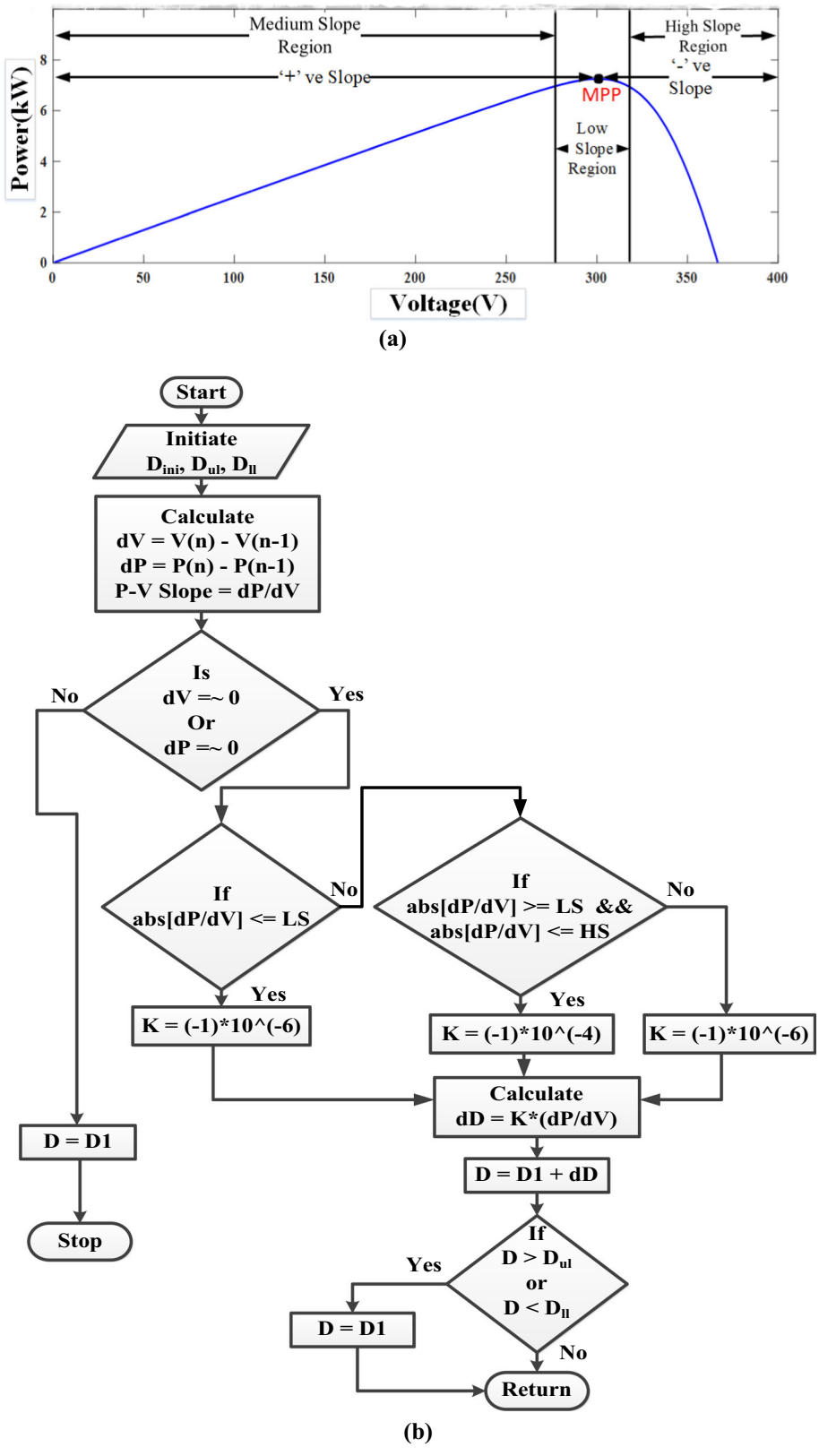


**Fig. 3** **a** Different regions of the P–V curve; **b** flowchart of the proposed MPPT technique

change in duty cycle d*D* at a high-slope region leads to a huge change in power, and therefore, d*D* should be smaller in this region. Therefore, the value of *K* will be different for each region and is given in the flow diagram, i.e., for low

and high-slope regions, it is $-1 \times 10^{-6}$ and for medium-slope region, it is $-1 \times 10^{-4}$. Now, the changes in duty cycle d$D$ are added to the previous duty cycle $D$ in every iteration and the change in power d$P$ is also monitored continuously.

$$D = D1 + \mathrm{d}D \tag{8}$$

## DC Bus Voltage and Active Power Flow Control

The voltage across the DC bus capacitor will be controlled by controlling the power injected to the AC system by the inverter. This can be done on the principle that the current drawn from the boost converter $I_{in}$ should be equal to the current delivered to the AC grid side through VSI i.e., $I_{out}$. Then, the voltage across the capacitor can be maintained at the desired level. The control scheme can be explained with the help of Fig. 4a, b. The DC bus voltage $V_{DC}$ can be controlled by using a PI controller which generates the reference current magnitude—to be injected into the AC system.

The voltage $V_{DC}$ depends upon the difference between $I_{in}$ and $I_{out}$ as follows:

If $I_{in} < I_{out}$, then $\rightarrow V_{DC} < V^*_{DC} \rightarrow I_{ref}$ should decrease.

If $I_{in} > I_{out}$, then $\rightarrow V_{DC} > V^*_{DC} \rightarrow I_{ref}$ should increase.

If $I_{in} = I_{out}$, then $\rightarrow V_{DC} = V^*_{DC} \rightarrow I_{ref}$ should remain constant.

Here, $V^*_{DC}$ is the reference DC bus voltage and $I_{ref}$ is the current reference generated by the PI controller and it is to be tracked by the VSC to control the active power injected to the AC system. By using hysteresis current control (HCC) scheme [24], $I_{ref}$ can be tracked to regulate the active power flow so that the voltage across DC bus capacitor can be maintained at desired magnitude. Using dqo to abc reference frame theory, the three-phase reference currents are generated from $I_{ref}$ [24]. PLL is used to get the exact phases in which the three-phase reference currents should be generated. The firing pulses are generated using actual and reference currents [24].

## Results and Discussion

The performance of the proposed scheme has been compared with the existing P&O method in two different modes, namely stand-alone mode and grid-connected mode.

(1) Stand-alone Mode of SECS.

To investigate the functioning of the new MPPT technique and to compare it with that of the P&O method, MATLAB/Simulink simulation study is carried out. An array consisting 10 series modules and 40 parallel strings of photovoltaic model TDB156x156-60-P 225 W was simulated. The complete rating of the considered PV array used in this study is as follows. Sun Earth Solar Power PV array model is considered for the implementation in MATLAB/Simulink. The ratings of the considered PV array are $10 \times 40$ modules of each 225 W, total PV array voltage of 370 V, a peak power of 90 kW at 1000 W/m$^2$ irradiance.

In this mode, the DC power is utilized after tracking the MPP using boost converter and the load is having a fixed impedance of 20 Ω and therefore, conversion of DC into AC is not required. The converter switching frequency is kept 5 kHz, converter inductor is 50 mH, and the capacitor is 4 mF. Next are the two cases considered for the verification of the proposed MPPT scheme in stand-alone mode.

*Change in irradiance* To show the impact of change in irradiance, a step change in the value of irradiance is made from 700 to 800 W/m$^2$ at t = 0.2 s as depicted in Fig. 5a. The temperature is kept constant at 25 °C. Figure 5b, c show the comparison of voltages and powers between conventional P&O and proposed MPPT techniques, respectively, for changed irradiance and at a constant temperature. It is found that the rise time and settling time of voltage and power of both the techniques are nearly equal and the steady-state values of voltages and powers for both the techniques are the same. However, both the plots for the proposed technique give lesser oscillations.

*Change in temperature* To show the impact of change in temperature, a step change in the value of temperature is made from 40 to 25 °C at t = 0.3 s as depicted in Fig. 6a. The irradiance is kept constant at 800 W/m$^2$. Figure 6b, c show the comparison of voltages and powers between

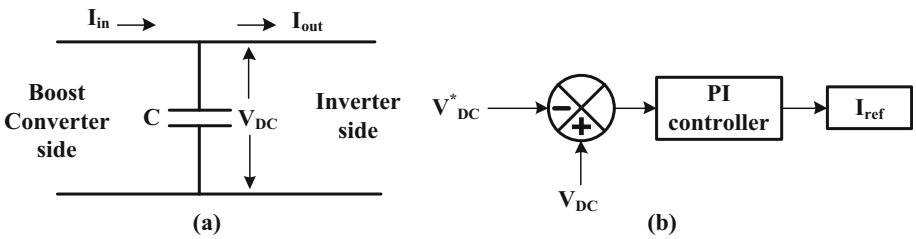


**Fig. 4** **a** DC bus capacitor; **b** DC bus voltage control using PI controller

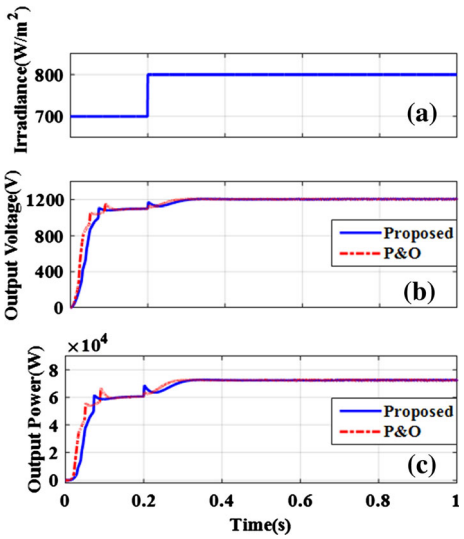


**Fig. 5** Comparison of P&O and proposed MPPT techniques for stand-alone mode with change in irradiance **a** irradiance, **b** converter output voltage, **c** power

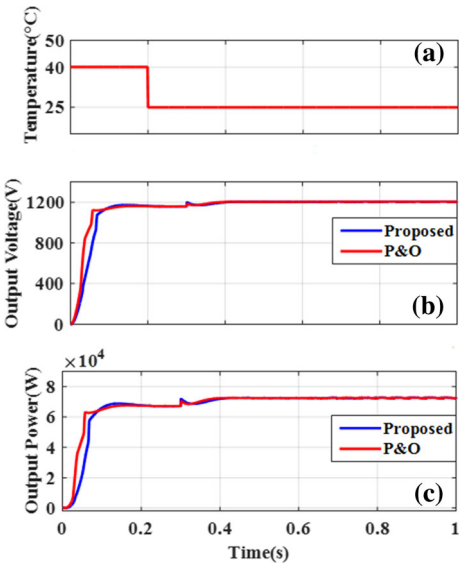


**Fig. 6** Comparison of P&O and proposed MPPT techniques for stand-alone mode with change in temperature **a** temperature, **b** converter output voltage, **c** power

conventional P&O and proposed MPPT techniques, respectively, for change in temperature and at a constant irradiance. It is, again, found that the rise time and settling

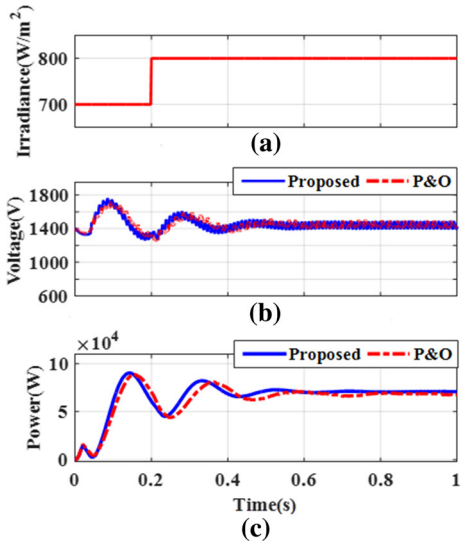


**Fig. 7** Comparison of P&O and proposed MPPT techniques for grid-connected mode with change in irradiance **a** irradiance, **b** converter output voltage, **c** power

time of voltage and power of both the techniques are nearly equal and the steady-state values of voltages and powers for both the techniques are the same. Though the proposed scheme gives lesser oscillations, the overshoot is slightly more.

For better understanding and comparison in stand-alone mode, the outcome of both the techniques is given in Table 1.

(2) AC grid-connected mode of SECS.

In this mode, the circuit is simulated as per the block diagram shown in Fig. 2. The AC load is considered to be parallel RLC load having R = 10Ω, L = 15 mH, and C = 470 μF with 0.84 pf lagging. The DC bus capacitor is initially charged to 1400 V to avoid high transient currents. The grid rms voltage is 400 V L–L. The grid interfacing inductance is 0.1 mH. The steady-state value of the DC bus voltage is 1440 V.

The performance is investigated by changing the irradiance from 700 to 800 W/m$^2$ at time 0.2 s—similar to that of stand-alone mode. The inverter is operated in active power injection mode with the help of a hysteresis current controller [24]. From Fig. 7, we can observe that the SECS

**Table 1** Comparison in stand-alone mode

| Parameter | P&O technique | Proposed technique |
|---|---|---|
| DC bus voltage | Attained steady-state value without error | Attained steady-state value without error |
| Steady-state power | Attained MPP without any error | Attained MPP without any error |
| Rise time | Slightly more when compared | Slightly less when compared |
| Settling time | Comparatively more | Comparatively less |
| Overshoots | More no. of overshoots compared to the proposed technique | Less no. of overshoots compared to P&O technique |

**Table 2** Comparison in grid-connected mode

| Parameters | P&O technique | Proposed technique |
|---|---|---|
| DC bus voltage | Attained steady-state value without error | Attained steady-state value without error and with slight oscillations |
| Steady-state power | Attained MPP with some deviations throughout the response | Attained MPP and settled at a constant value |
| Rise time | Comparatively more | Comparatively less |
| Settling time | Comparatively more | Comparatively less |
| Overshoots | No. of overshoots are more | No. of overshoots are less |

takes more time in achieving the steady state as compared to that of stand-alone mode. When the irradiance is changed from 700 to 800 W/m$^2$ at t = 0.2 s, the SECS was not able to achieve steady state for irradiance of 700 W/m$^2$ due to transient period, but it achieved the same for 800 W/m$^2$ in about 0.6 s. Figure 7a illustrates the irradiance, Fig. 7b shows the DC bus voltage, and Fig. 7c represents the power extracted from SECS which is supplied to the AC system. It is also evident that the maximum power can be extracted from the solar panel at a given irradiance, i.e., at an irradiance of 800 W/m$^2$ the maximum power of 72 kW is extracted, and it is shown in Fig. 7c. Now, for comparison purposes, Table 2 includes different parameters for both the schemes.

## Conclusion

According to the change in irradiance and temperature, there will be a change in the I–V curve, P–V curve, and maximum power point. Therefore, the operating voltage of the PV array needs to be modified to extract the maximum power. In other words, the impedance offered by the converter should be varied in accordance with that of the PV array. To change this offered impedance, the duty cycle of the converter needs to be varied accordingly. Different aspects of the solar energy conversion system have been discussed in detail, and a new MPPT technique has been proposed. In stand-alone mode, the new technique successfully tracks the MPP down and gives comparable results to that of the P&O technique and the oscillations in the proposed technique are lesser than that of the P&O scheme. In grid-connected mode, the proposed scheme gives improved results and provides lesser oscillations in output and has improved rise time and settling time. Overall, the detailed study of the solar energy conversion system and the proposed scheme will surely be interesting and helpful to the readers.

## References


1. A. Skumanich, P. Mints, "Micro-grid and DG expansion: key role of storage, projected global demand," in *Conf. Rec. IEEE Photovolt. Spec. Conf.*, vol. 2016-Nov (2016) pp. 1865–1868
2. S. Jain, V. Agarwal, An integrated hybrid power supply for distributed generation applications fed by nonconventional energy sources. IEEE Trans. Energy Convers. **23**(2), 622–631 (2008)
3. N. Kumar, I. Hussain, B. Singh, B.K. Panigrahi, Normal harmonic search algorithm-based MPPT for solar PV system and integrated with grid using reduced sensor approach and PNKLMS algorithm. IEEE Trans. Ind. Appl. **54**(6), 6343–6352 (2018)
4. H. Suryoatmojo et al., "Design of MPPT based fuzzy logic for solar-powered unmanned aerial vehicle application," in *ICEAST 2018-4th International Conference on Engineering, Applied Sciences and Technology: Exploring Innovative Solutions for Smart Society*, (2018)
5. K. Kumar, R.N. Babu, K.R. Prabhu, Design and analysis of RBFN-based single MPPT controller for hybrid solar and wind energy system. IEEE Access **5**, 15308–15317 (2017)
6. N. Pachaivannan, R. Subburam, U. Ramkumar, P. Kasinathan, Crowded plant height optimisation algorithm tuned maximum power point tracking for grid integrated solar power conditioning system. IET Renew. Power Gener. **13**(12), 2137–2147 (2019)
7. H. Li, D. Yang, W. Su, J. Lu, X. Yu, An overall distribution particle swarm optimization MPPT algorithm for photovoltaic system under partial shading. IEEE Trans. Ind. Electron. **66**(1), 265–275 (2019)
8. A.K. Singh, S. Kumar, B. Singh, Solar PV energy generation system interfaced to three phase grid with improved power quality. IEEE Trans. Ind. Electron. **67**(5), 3798–3808 (2020)
9. S. Kumar, B. Singh, "Seamless transition of three phase microgrid with load compensation capabilities," in *2017 IEEE Industry Applications Society Annual Meeting* (2017), pp. 1–9
10. M. Chikh, M. Haddadi, A. Mahrane, A. Malek, Assessment of the diffuse component of the global horizontal solar radiation for different solar altitude ranges. Case study: Oran (Algeria). IET Renew. Power Gener. **13**(4), 640–649 (2019)
11. M. Heidari Kapourchali, M. Sepehry, V. Aravinthan, Multivariate spatio-temporal solar generation forecasting: a unified approach to deal with communication failure and invisible sites. IEEE Syst. J. **13**(2), 1804–1812 (2019)
12. M. Feifel et al., Direct growth of III-V/Silicon triple-junction solar cells with 19.7% efficiency. IEEE J. Photovolt. **8**(6), 1590–1595 (2018)
13. B. Qi, J. Wang, Fill factor in organic solar cells. Phys. Chem. Chem. Phys. **15**(23), 8972–8982 (2013)
14. T. Esram, P.L. Chapman, Comparison of photovoltaic array maximum power point tracking techniques. IEEE Trans. Energy Convers. **22**(2), 439–449 (2007)

15. A. Safari, S. Mekhilef, Simulation and hardware implementation of incremental conductance MPPT with direct control method using cuk converter. IEEE Trans. Ind. Electron. **58**(4), 1154–1161 (2011)
16. D. P. Hohm, M. E. Ropp, "Comparative study of maximum power point tracking algorithms using an experimental, programmable, maximum power point tracking test bed," in *Conference Record of the IEEE Photovoltaic Specialists Conference* (2000), pp. 1699–1702
17. M. Bodur, M. Ermis, "Maximum power point tracking for low power photovoltaic solar panels," in *Mediterranean Electrotechnical Conference-MELECON* (1994), vol. 2
18. R. F. Coelho, F. M. Concer, D. C. Martins, "A MPPT approach based on temperature measurements applied in PV systems," in *2010 IEEE International Conference on Sustainable Energy Technologies, ICSET 2010* (2010)
19. N. Femia, G. Petrone, G. Spagnuolo, M. Vitelli, Optimization of perturb and observe maximum power point tracking method. IEEE Trans. Power Electron. **20**(4), 963–973 (2005)
20. L. M. Satapathy, A. Harshita, M. Saif, P. K. Dalai, S. Jena, "Comparative analysis of boost and buck-boost converter in photovoltaic power system under varying irradiance using MPPT," in *Proceedings of the International Conference on Inventive Communication and Computational Technologies, ICICCT 2018* (2018), pp. 1828–1833
21. R. Patii, H. Anantwar, "Comparitive analysis of fuzzy based MPPT for buck and boost converter topologies for PV application," in *Proceedings of the 2017 International Conference On Smart Technology for Smart Nation, SmartTechCon 2017* (2017), pp. 1479–1484
22. Alexis De Vos, The fill factor of a solar cell from a mathematical point of view. Sol. Cells **8**(3), 283–296 (1983)
23. B. J. Saharia, M. Manas, S. Sen, "Comparative study on buck and buck-boost DC-DC converters for MPP tracking for photovoltaic power systems," in *Proceedings-2016 2nd International Conference on Computational Intelligence and Communication Technology, CICT 2016* (2016), pp. 382–387
24. O.H. Gupta, M. Tripathy, V.K. Sood, Islanding detection scheme for converter-based DGs with nearly zero non-detectable zone. IET Gener. Transm. Distrib. **13**(23), 5365–5374 (2019)